JPE 9-3-3

An On-line Rotor Resistance Estimator for Induction Machine Drives

Chun-Ki Kwon†

†Dept. of Medical IT Engeering, Soonchunhyang University, Korea

ABSTRACT

Rotor resistance variation due to changing rotor temperature is a significant issue in the design of induction motor controls. In this work, a new on-line rotor resistance estimator is proposed based on an alternate *qd* induction machine model which provides better mathematical representation of an induction machine than the classical *qd* model (which uses constant parameters). This is because the former simultaneously includes leakage saturation, magnetizing path saturation, and distributed circuit effects in the rotor conductors. The comparisons via computer simulation studies show the ability of the proposed estimator to accurately track rotor resistance variation. For the experimental studies, due to the difficulty in measuring the actual rotor resistance, comparison of the controller performance using the proposed estimator, the classical *qd* model based estimator, and no estimator is made.

Keywords: Induction machine model, Control strategy, Rotor resistance estimator

1. Introduction

The variation of rotor resistance due to rotor temperature can cause significant performance degradation unless it is taken into account. Thus, consideration of rotor resistance variation has been a significant issue in control design, particularly in the case of optimal controls [1-7].

Numerous rotor resistance estimators have been proposed in the literature. Most of these estimators [1-12] are based on the classical *qd* induction machine model (CQDM) whose deficiencies have long been noted. These deficiencies include failure to represent leakage saturation, magnetizing path saturation, and distributed system effects in the rotor conductors [13-18]. None of these rotor resistance estimators have been specifically designed for conditions under which the magnetizing flux level varied significantly. If the magnetic operating point does not vary greatly, this is not an issue. For example, suppose a rotor resistance estimator based on the CQDM is used in the context of a field-oriented control in which the flux level is constant. Under these conditions, the estimators [1-12] should be effective. However, if a maximum torque per amp (MTPA) control strategy is used wherein the flux level varies [19], the performance of an estimator based on the CQDM is questionable. In fact, the estimators described in [1-12] have not been demonstrated in conditions where the flux varies significantly.

Recently, an alternate *qd* model (AQDM) was proposed [20]. This model simultaneously includes leakage saturation, magnetizing saturation, and the ability to represent distributed effects in the rotor conductors. The model

Manuscript received October 28, 2008; revised Feb. 10, 2009
†Corresponding Author: chunkikwon@sch.ac.kr
Tel:+82-41-530-3091, Fax:+82-41-530-3085, Soonchunhyang Univ.
Dept. of Medical IT Eng., Soonchunhyang Univ., Korea

has been shown to yield accurate predictions of machine behavior at both the fundamental and switching frequencies [19-22].

In this work, a new on-line rotor resistance estimator is proposed based on the AQDM, thus taking the deficiencies of the CQDM into consideration. Regardless of changing operating conditions, the proposed AQDM based estimator is shown to predict rotor resistance with good accuracy. The performance of the proposed estimator is demonstrated using both computer simulations and laboratory experiments. Since the actual rotor resistance is unknown and cannot be directly measured, performances of the MTPA control strategy in [19] using the AQDM based rotor resistance estimator, the CQDM based estimator, and no estimator were compared to indirectly demonstrate the good performance of the proposed rotor resistance estimator.

2. Notation

In this work, electrical rotor position is designated θ_r and electrical rotor speed ω_r. These quantities are related to the mechanical rotor position θ_{rm} and mechanical rotor speed ω_{rm} by a factor of $P/2$ where P is the number of poles.

This work will make use of a transformation of variables to both the rotor and synchronous reference frames. The transformation of stator or inverter quantities may be expressed

$$\begin{bmatrix} f_{qy}^{x} & f_{dy}^{x} & f_{0y}^{x} \end{bmatrix}^T = K_s^x(\theta) \begin{bmatrix} f_{qy}^{x} & f_{dy}^{x} & f_{0y}^{x} \end{bmatrix}^T \quad (1)$$

where 'y' may be 's' for stator, 'i' for inverter , or 'm' for magnetizing, 'f' may be a 'v' for voltage, 'i' for current, or 'λ' for flux linkage, and

$$K_s^x(\theta) = \frac{2}{3} \begin{bmatrix} \cos(\theta) & \cos(\theta - 2\pi/3) & \cos(\theta + 2\pi/3) \\ \sin(\theta) & \sin(\theta - 2\pi/3) & \sin(\theta + 2\pi/3) \\ 1/2 & 1/2 & 1/2 \end{bmatrix}^T \quad (2)$$

The superscript 'x' will denote frame of reference. In a break with the usual notation, omission of a superscript will designate the rotor reference frame in which $\theta = \theta_r$. This is done for notational simplicity since most quantities used herein are expressed in the rotor reference frame. Setting 'x' to 'e' will denote the synchronous reference frame. A similar transformation is used for rotor variables with the exception that θ is replaced by $\theta - \theta_r$ in (1)–(2).

A related transformation used herein is the q- and d-axis inverter current transformation given by

$$\begin{bmatrix} i_{qi}^{x} & i_{di}^{x} \end{bmatrix}^T = K_{s,i}^{x}(\theta) \begin{bmatrix} i_{ai} & i_{bi} \end{bmatrix}^T \quad (3)$$

where

$$K_{s,i}^{x}(\theta) = \frac{2}{\sqrt{3}} \begin{bmatrix} \cos(\theta - \pi/6) & \sin(\theta) \\ \sin(\theta - \pi/6) & -\cos(\theta) \end{bmatrix} \quad (4)$$

This variation arises from the assumption that the sum of the inverter currents is zero. In a similar way, a transformation for the q- and d- axis inverter voltages may be expressed as

$$\begin{bmatrix} v_{qi}^{x} & v_{di}^{x} \end{bmatrix}^T = K_{s,v}^{x}(\theta) \begin{bmatrix} v_{abi} & v_{bci} \end{bmatrix}^T \quad (5)$$

where

$$K_{s,v}^{x}(\theta) = \frac{2}{3} \begin{bmatrix} \cos(\theta) & -\cos(\theta + 2\pi/3) \\ \sin(\theta) & -\sin(\theta + 2\pi/3) \end{bmatrix} \quad (6)$$

A more detailed discussion of reference frame theory and notation is set forth in [23].

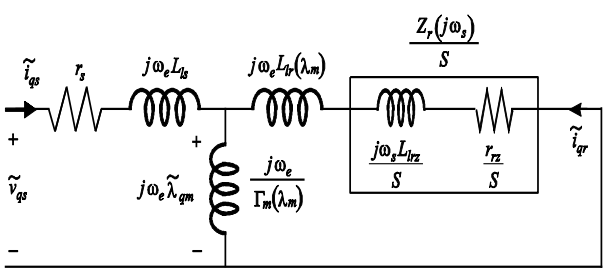

Fig. 1. Steady-state equivalent circuit of the AQDM model with rotor impedance represented as $r_{rz} + j\omega_s L_{lrz}$.

3. Alternate QD Induction Machine Model

The steady-state equivalent circuit representing the AQDM in [21] is shown in Fig. 1. Therein, the AQDM has been modified slightly in that the rotor resistance corresponds to a 1st order rather than an arbitrary order network. This is possible because the model is only being used to predict fundamental frequency behavior at low slip values [24]. As can be seen, the rotor impedance, $Z_r(j\omega_s)$, is separated into a real and imaginary part, which are denoted r_{rz} and $j\omega_s L_{lrz}$, respectively, ω_s is defined as $\omega_e - \omega_r$, λ_m is equal to $\sqrt{2}\left|\tilde{\lambda}_{qm}\right|$, and slip S is defined as $(\omega_e - \omega_r)/\omega_e$. Additional details on the model and nomenclature are set forth in [20]-[21].

The functional forms of machine parameters for AQDM parameters, which are stator and rotor leakage inductances, the absolute inverse magnetizing inductance, and the rotor admittance, are as follows:

$$L_{ls} = l_{s1} \text{ (a constant)} \tag{7}$$

$$L_{lr} = l_{r1} + l_{r2} / \left(1 + (l_{r3} \cdot \lambda_m)^{l_{r4}}\right) \tag{8}$$

$$\Gamma_m(\lambda_m) m_1 - m_2 \cdot \lambda_m + e^{m_3(\lambda_m - m_4)} + e^{m_5(\lambda_m - m_6)} \tag{9}$$

$$Y_r(s) = \frac{1}{Z_r(s)} = \frac{y_{a1}}{y_{\tau 1}s + 1} + \frac{y_{a2}}{y_{\tau 2}s + 1} + \frac{y_{a3}}{y_{\tau 3}s + 1} \tag{10}$$

Table 1 Resultant parameters

$L_{ls}(\cdot)$			$\Gamma_m(\cdot)$		
l_{s1}	9.1e-4	H	m_1	6.79e0	H^{-1}
$L_{lr}(\cdot)$			m_2	6.62e-1	$(H \cdot V \cdot s)^{-1}$
l_{r1}	1.4e-4	H	m_3	5.03e0	$(H \cdot V \cdot s)^{-1}$
l_{r2}	4.2e-3	H	m_4	1.85e0	$V \cdot s$
l_{r3}	7.35e-1	$(V \cdot s)^{-1}$	m_5	8.68e-1	$(H \cdot V \cdot s)^{-1}$
l_{r4}	2.59e0		m_6	1.29e-1	$V \cdot s$
$Y_r(\cdot)$					
y_{a1}	5.65e0	$(\Omega)^{-1}$	$y_{\tau 1}$	3.21e-2	s/rad
y_{a2}	4.40e-2	$(\Omega)^{-1}$	$y_{\tau 2}$	4.78e-4	s/rad
y_{a3}	3.17e-3	$(\Omega)^{-1}$	$y_{\tau 3}$	8.76e-8	s/rad

The test system for this work utilizes a 4-pole, 460 V, 50 Hp, 60 Hz, delta-connected squirrel cage induction machine. Using the methods set forth in [22], the machine parameters of the AQDM for the test induction machine are listed in Table 1.

4. Sensitivity Study of Induction Machine Temperature Variation

In order to justify the need for a rotor resistance estimator, consider the performance of an induction machine with an MTPA control strategy. Using the procedure set forth in [19], the MTPA control laws derived for the test induction machine may be expressed as

$$I_s^*(T_e^*) = 0.102 \cdot T_e^* - 6.41 \cdot T_e^{*\,0.0110} + 7.79 \cdot T_e^{*\,0.152} \tag{11}$$

$$\omega_s^*(T_e^*) = 1.27 + 0.00443 \cdot T_e^{*\,1.15} \tag{12}$$

Fig. 2 illustrates the effect of temperature on the electromagnetic torque at a particular operating condition using the control law (11)-(12) in the lab experiment. Therein, the test induction machine is driven at a speed of 900 rpm at a torque command of 150 Nm. This corresponds to the inverter current command I_s = 61.58 A and the slip frequency command ω_s = 2.6829 rad/s. The torque (hereinafter, called torque estimate) was estimated by a torque estimator, which was shown to be highly accurate when an induction machine is rotating at moderate to high speeds [25-26]. Trace (a) illustrates the measured electromagnetic torque estimate versus surface temperature of a point on the stator of the test induction machine, which was measured using a Fluke 65 infrared thermometer. The time at which each data point was taken relative to the beginning of the study is designated $+X$ where X is the time in minutes. The torque estimate and the surface temperature of the test induction machine were measured every 5 minutes. It is shown in trace (a) that the variation of the measured electromagnetic torque estimate at the same operating condition is significant as stator temperature of the test induction machine rises. As can be seen, as the stator surface

temperature (and presumably rotor temperature) rises, the torque estimate increases, reaches a maximum, and then decreases. The rotor resistance at maximum torque point (near $43^{\circ}C$) corresponds to the effective rotor resistance (used to design the MTPA control law in (11)-(12)). At this point the measured torque estimate is very close to the commanded torque.

In the Fig. 2 trace (b), the measured torque estimate at the optimal slip frequency command, ω_s^*, in (12) is compared with two additional sets of torque estimate measurements taken at 110% and 90% times ω_s^*. At low temperatures where rotor resistance is smaller than the rotor resistance used to design the MTPA control strategy, the torque estimate measured at 90% times ω_s^* in (12) was larger and closer to the commanded torque. Then with $\omega_s = \omega_s^*$, it can also be seen that as the study proceeds in time, eventually the slip frequency command of 110% of ω_s^* yields the greatest torque estimate, which implies that the maximum torque per amp condition at ω_s^* in (12) is not achieved. However, for some temperature region, around $43^{\circ}C$, maximum torque per ampere condition is in fact achieved at the estimate optimal slip frequency command ω_s^* defined by (12). These observations lead to the conclusion that to avoid the degradation in the performance of the MTPA control strategy due to rotor resistance variation, the actual rotor resistance should be estimated and taken into account in the design of the MTPA control strategy.

5. Derivation of the AQDM Based Rotor Resistance Estimator

The previous section justifies the need for estimating the actual varying rotor resistance during operation. In this section, a new on-line rotor resistance estimator is proposed based on the AQDM. This AQDM based rotor resistance estimator will be shown to predict the actual rotor resistance with high accuracy regardless of operating conditions.

The rotor resistance estimator can be derived from the AQDM steady-state equivalent circuit shown in Fig. 1, where rotor resistance can be treated as a lumped parameter within the normal control range of the slip frequency [24]. From stator measurements, the stator input impedance $\hat{Z}_{qs}$ can be observed. By equating the measured value to the value corresponding to the stator equivalent circuit, the stator impedance entering the input terminal may be expressed as

$$\hat{Z}_{qs} = r_s + j\omega_e L_{ls} + Z_{ag} \tag{13}$$

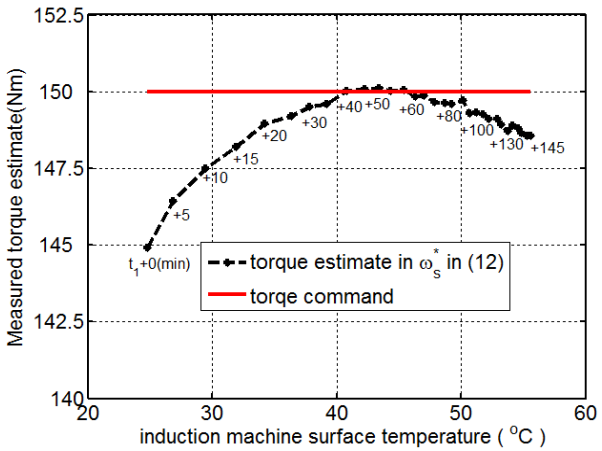

(a) Measured torques estimates at optimal slip frequency, ω_s^*.

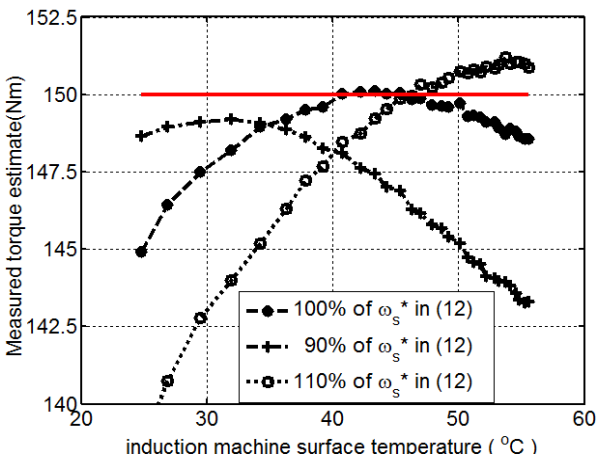

(b) Maximum torque per ampere condition.

Fig. 2. Effect of temperature on torque with $T_e^* = 150(\mathrm{Nm})$ using the MTPA control strategy based on (11)-(12) ω_s^*.

The superscript ' ^ ' in $\hat{Z}_{qs}$ is used to indicate a measured value. From (13), the impedance entering the air-gap, Z_{ag}, may be computed as

$$Z_{ag} = \hat{Z}_{qs} - (r_s + j\omega_e L_{ls}) \tag{14}$$

Since Z_{ag} in (14) has parallel circuit elements, it is conveniently expressed as an admittance

$$Y_{ag}(r_{rz}) = \frac{1}{Z_{ag}} = \frac{-j\Gamma_m(\hat{\lambda}_m)}{\omega_e} + \frac{1}{Z_{RB}} \tag{15}$$

where Z_{RB} is the impedance of the rotor branch defined as

$$Z_{RB} = j\omega_e L_{lr}(\hat{\lambda}_m) + r_r/S + j\,\omega_s L_{lrz}/S \tag{16}$$

From (16), the estimated rotor resistance may be expressed

$$\hat{r}_{rz} = \frac{\omega_s}{\omega_e} \cdot \mathrm{Re}\{Z_{RB}\} \tag{17}$$

In (16)-(17), the superscript ' ^ ' in $\hat{r}_{rz}$ serves as a reminder that this is the estimated value; Similarly, $\hat{\lambda}_m$ will be the estimated magnitude of the magnetizing flux (the estimate of $\hat{\lambda}_m$ will be discussed later in this section). By the substitution of (14) into (15) and algebraic manipulation, Z_{RB} can be also expressed

$$Z_{RB} = \left((\hat{Z}_{qs} - r_s - j\omega_e L_{ls})^{-1} + \frac{j\Gamma_m(\hat{\lambda}_m)}{\omega_e} \right)^{-1} \tag{18}$$

Fig. 3 depicts the block diagram of the proposed AQDM based rotor resistance estimator based on (17)-(18).

Therein, the stator input impedance $\hat{Z}_{qs}$ is readily obtained from the measured *a*- and *b*- phase inverter currents, $\hat{i}_{ai}$ and $\hat{i}_{bi}$, and the measured line-to-line inverter voltages, $\hat{v}_{abi}$ and $\hat{v}_{bci}$. These measured inverter quantities are transformed to $\hat{i}^e_{qi}$ and $\hat{i}^e_{di}$ using (4), and, $\hat{v}^e_{qi}$ and $\hat{v}^e_{di}$ using (6), respectively. These quantities are filtered by two cascaded first order low pass filters (LPF) to remove switching noise. The time constant of each LPF is 8 ms in the test system. Recall that the phasor representation of a quantity in an asynchronous reference frame is related to its *q*- and *d*- axis components in the synchronous reference frame by

$$\sqrt{2}\tilde{f}_{qi} = f^e_{qi} - jf^e_{di} \tag{19}$$

where ' f ' may be a ' v ' for voltage, ' i ' for current, or ' λ ' for flux linkage. Using (19), inverter currents and voltage phasors $\tilde{i}_{qi}$ and $\tilde{v}_{qi}$, respectively, are obtained. Since the test induction machine is delta-connected, the resulting stator phasors are related to the inverter phasors by

$$\tilde{v}_{qs} = \sqrt{3} \cdot \tilde{v}_{qi} \cdot e^{-j\pi/6} \tag{20}$$

$$\tilde{i}_{qs} = \frac{1}{\sqrt{3}} \cdot \tilde{i}_{qi} \cdot e^{-j\pi/6} \tag{21}$$

where $j = \sqrt{-1}$. Next, the measured stator input impedance $\hat{Z}_{qs}$ may be found using

$$\hat{Z}_{qs} = \frac{\tilde{v}_{qs}}{\tilde{i}_{qs}} \tag{22}$$

The possibility of division by zero and poor signal-to-noise ratio under low voltage conditions due to noise or measurement error in (22) must be taken into consideration. To this end, (22) is modified as

$$\hat{Z}_{qs} = \frac{\alpha\tilde{v}_{qs} + (1-\alpha)Z_{qs0}I_{sT}}{\alpha\tilde{i}_{qs} + (1-\alpha)I_{sT}} \tag{23}$$

Where

$$\alpha = \min(\alpha_v, \alpha_i) \tag{24}$$

In (24), α_v and α_i are defined as

$$\alpha_v = \begin{cases} 1 & if \ \left|\tilde{v}_{qs}\right| \geq V_{sT} \\ \left|\tilde{v}_{qs}\right| / V_{sT} & else \end{cases} \tag{25}$$

and

$$\alpha_i = \begin{cases} 1 & if \ \left|\tilde{i}_{qs}\right| \geq I_{sT} \\ \left|\tilde{i}_{qs}\right| / I_{sT} & else \end{cases} \tag{26}$$

, respectively. In (25)-(26), V_{sT} and I_{sT} are the stator voltage threshold and the stator current threshold which are set to the level at which measurement deteriorates. In the test system, they were set to 5% of each corresponding rated value. In (23), the term Z_{qs0} represents an approximation of the stator impedance under low current conditions. Z_{qs0} can be calculated from the AQDM assuming zero flux level (since the current is small) using the present estimated value of rotor resistance and rotor speed.

Another important part of the control is the estimate of the flux level, which is needed because the absolute inverse magnetizing inductance Γ_m in (18) is a function of $\hat{\lambda}_m$. Once $\tilde{v}_{qs}$ and $\tilde{i}_{qs}$ are obtained, the estimate of the peak amplitude of magnetizing flux linkage $\hat{\lambda}_m$ is readily calculated using

$$\hat{\lambda}_m = \sqrt{2}\,\frac{\left|\tilde{v}_{qs} - \left(r_s + j \cdot \omega_e \cdot L_{ls}\right)\tilde{i}_{qs}\right|}{\omega_e} \tag{27}$$

Once the estimated flux level is determined, it may be used in conjunction with (17)-(18) to find the unconditioned rotor resistance estimate $\hat{r}_{rz}$.

Even though the AQDM based rotor resistance estimator is based on the steady-state equivalent circuit, there is no performance degradation of the proposed estimator in the transient period because of the relatively big thermal time constant in the rotor bar compared to the motor electric time constant. However, it is desirable to prevent transient behaviors in case of operating condition changes from influencing the estimator in an undesirable way. This is accomplished using a slew rate limiter (SRL) to limit the rate of change of the estimated rotor resistance to values between $\alpha_{\min}$ and $\alpha_{\max}$. In the test system, these were set to -5 $m\Omega/s$ and 5 $m\Omega/s$, respectively.

Due to the switching noise inherent in a current controlled induction machine drive used in this work [19], the estimated rotor resistance is also filtered through a low-pass filter. Since the rotor resistance will normally vary slowly, this time constant, τ_{rrz}, can be made quite large. In the experimental implementation, a value of 1.5 s is used. Finally, to keep the estimated rotor resistance in a reasonable range, the resulting estimated rotor resistance is bounded between $r_{rz,\min}$ and $r_{rz,\max}$. For the test system, these were selected to be $0.09\,\Omega$ and $0.35\,\Omega$, respectively.

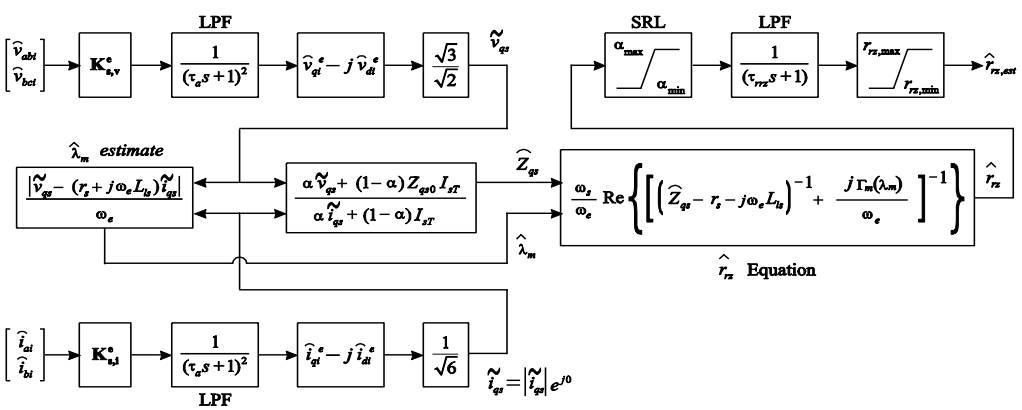

Fig. 3. Block diagram of the proposed AQDM based rotor resistance estimator.

6. Validation of the AQDM Based Rotor Resistance Estimator

The performance of the proposed AQDM based rotor resistance estimator was investigated using both a computer simulation and a laboratory experiment. The configuration for the induction machine drive is depicted in Fig. 4. Since the actual rotor resistance is unknown and cannot be directly measured, a computer simulation study was used to determine if the estimator would track a time-varying rotor resistance. For the computer simulation study, the AQDM with the parameters listed in Table 1 was used for a truth model. The rotor resistance was initially set to 0.11 Ω and varied to simulate rotor temperature increase. Since the rotor circuits in AQDM are represented by the rotor admittance where rotor resistance is implicit, the rotor admittance is varied rather than the rotor resistance itself. To this end, the dc component of the rotor admittance specified in (10) is selected, which is $Y_r(0)$. Unfortunately, this method also causes the frequency dependent rotor inductance, $L_{lrz}(j\omega_s)$, to change as well. Nevertheless, this approach is taken for convenience since the most significant validation step will be experimental. In this study, $Y_r(0)$ is assumed to vary as

$$Y_r(0) = 7.0 \cdot \left(0.7 + 0.6e^{-0.005t}\right) \tag{28}$$

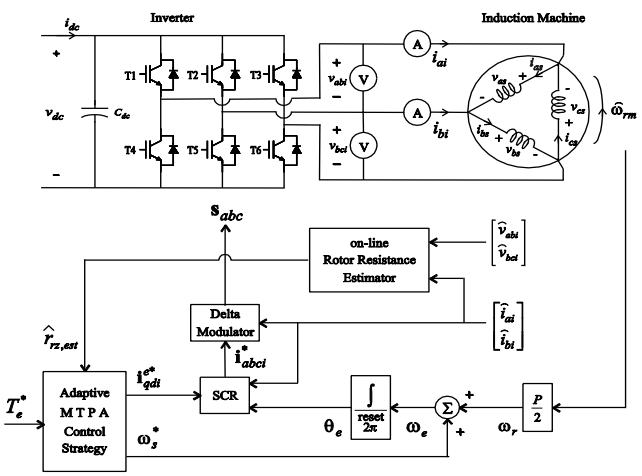

Fig. 4. The configuration of the voltage source current controller d inverter-fed induction machine drive used.

The exponential function is selected to emulate the trend of rotor resistance variation which increases quickly at the beginning of the induction machine operation and then increases more slowly as the temperature approaches steady-state condition. The induction machine was assumed to be driven at a speed of 900 rpm.

This study includes the performance of the proposed AQDM based rotor resistance estimator during step changes in operating conditions. The variation of actual rotor resistance is used in accordance with (28). In addition, during the study, three operating conditions are generated by the MTPA control law in (11)-(12). Initially, the test induction machine was operated at a moderate torque command of 130 Nm. After 300 s, the torque command was reduced to 20 Nm. Finally, at t =600 s, the torque command was stepped up to 180 Nm.

Based on this test condition, the performance of the proposed AQDM based rotor resistance estimator for this study is shown in Fig. 5. Trace (a) shows the comparison between actual rotor resistance and the estimated rotor resistance and trace (b) depicts the errors between the two. It is shown that the proposed AQDM based rotor resistance estimator predicts the rotor resistance with high accuracy regardless of operating conditions and that the performance degradation of the AQDM based rotor resistance estimator in the transient period is not significant (herein, less than 4% error).

For the purpose of experimental validation, an indirect approach must be used since it is difficult to directly measure the actual rotor resistance of the test induction machine. In particular, the performance of this AQDM based rotor resistance estimator is investigated by comparing the performances of three MTPA control strategies. The first MTPA control strategy is static in the sense that it is based on a constant rotor resistance. This static MTPA control law is specified by (11)-(12). The other two MTPA control strategies are adaptive and explicitly include rotor resistance as a part of the control law as in [24]. Using the same procedure set forth in [24], the control law for the test machine may be expressed as

$$I_s^*\left(T_e^*\right) = 0.102 \cdot T_e^* - 6.41 \cdot T_e^{*\,0.0110} + 7.79 \cdot T_e^{*\,0.152} \tag{29}$$

$$\omega_s^*\left(T_e^*, r_{rz}^*\right) = 7.22 \cdot r_{rz}^{*\,0.9998} + 0.025 \cdot r_{rz}^{*1.00} \cdot T_e^{*\,1.15} \quad (30)$$

With this adaptive MTPA control law, the second MTPA control strategy employs the proposed AQDM based rotor resistance estimator to determine the resistance, r_{rz}, in (30) while the third makes use of the rotor resistance estimator based on the CQDM using the parameters listed in Table 2. These parameters were determined so as to achieve a best fit to the stator impedance over a variety of operating points.

Proper performance of the two adaptive MTPA control strategies relies on accurate knowledge of the rotor resistance selected. Thus, good performance of the adaptive MTPA control strategy demonstrates the performance of the rotor resistance estimator incorporated.

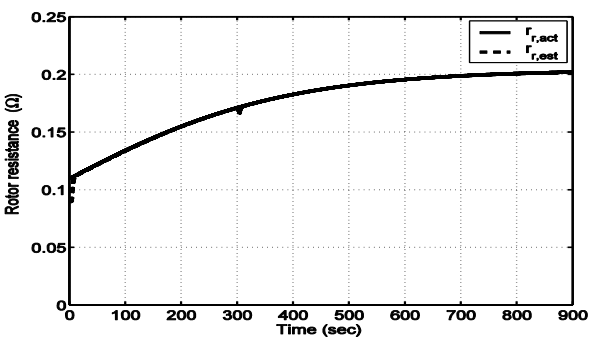

(a) Comparison of the estimated and the actual rotor resistance.

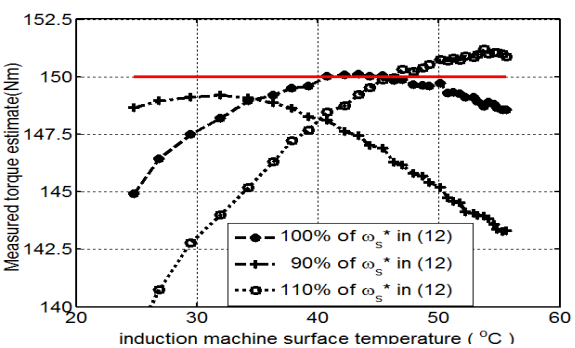

(b) % of normalized error between the estimated and the actual rotor resistance.

Fig. 5. Performance of rotor resistance estimator at different operating conditions.

Table 2 CQDM parameters

r_s	L_{ls}	L_{lr}	L_m	r_r
0.22 Ω	4.16 mH	4.16 mH	91.5 mH	0.159 Ω

Fig. 6 (a) compares the experimentally observed performances of the three MTPA control strategies under a particular operating condition. The test induction machine was driven at a speed of 900 rpm and the torque command was set to 150 Nm in all three cases. Measurements in this paper were partially made by waverunner xi digital storage oscilloscope and its accessories

As can be seen, the torque estimate produced by the adaptive MTPA control strategy which employs the proposed AQDM based rotor resistance estimator is closer to the torque command of 150 Nm than the torque estimate produced by the static MTPA control strategy. The torque estimate produced by the adaptive MTPA control strategy whose rotor resistance estimator is based on the CQDM generally performs worse than the static MTPA control strategy.

In Fig. 6 (b), two additional sets of torque estimate measurement are shown. In particular, measurements corresponding to the static MTPA control strategy at 0.9 and 1.1 times of the estimated optimal slip frequency commands given by (12) have been included. Therein, it can be observed that the torque estimate produced by the adaptive MTPA control strategy with the proposed AQDM based rotor resistance estimator incorporated is greater than the torque estimate measured at any slip frequency of the static MTPA control strategy. As can be seen, the adaptive MTPA control strategy with the CQDM based rotor resistance estimator does not satisfy the maximum torque per ampere condition. This indicates that the maximum torque per amp condition (refer to Fig. 2 b) is in fact achieved by the adaptive MTPA control strategy when the rotor resistance is estimated by the proposed AQDM based rotor resistance estimator.

In order to see if the observations of the study reported in Fig. 6 would hold over a variety of operating conditions, a second study was performed. In the second study, the

torque command was initially 25 Nm, then stepped sequentially to 50 Nm, 100 Nm, 150 Nm, and then finally 200 Nm, thereby exercising the machine from very low to rated torque at a given speed (herein, 900 rpm). Since an MTPA control is used, each change in torque command also causes a change in magnetizing flux.

As in Fig. 6 (b), Fig. 7 illustrates five sets of torque estimate measurements under all operating conditions selected. Therein, it is shown that the adaptive MTPA control strategy with the proposed AQDM based rotor resistance estimator produces the largest torque estimate. Conversely, the adaptive MTPA control strategy with the CQDM based rotor resistance estimator does not satisfy the maximum torque per amp condition over all torque commands selected. Thus, the proposed AQDM based rotor resistance estimator is superior to the CQDM based rotor resistance estimator.

Despite the improvements of the performance by the adaptive MTPA control strategy over the static MTPA control strategy, there exists deviation from the commanded torque in the case of the operation conditions where the torque commands are set to 25 Nm. At this point, the error in the open loop control is on the order of 5%. There are several explanations for this. First, at the low signal levels, the current sensor error becomes more significant. Secondly, again at low current levels, the rotor resistance estimator may not be as accurate as at higher current levels. Finally, again at very low current levels, the AQDM on which the control law is based may lose accuracy. All of these factors contribute to the approximately 5 % error.

The rotor resistance estimates by the proposed AQDM based rotor resistance estimator and the CQDM based rotor resistance estimator were compared in Fig. 8. It shows the estimated rotor resistances predicted by two rotor resistance estimators at a torque command of 150 Nm. Over a 2.5 hour period, the rotor resistance estimated by the proposed AQDM based rotor resistance estimator varies from $0.15\,\Omega$ to $0.19\,\Omega$ in an asymptotic fashion. The rotor resistance estimated by the CQDM based rotor resistance estimator varies from $0.14\,\Omega$ to $0.175\,\Omega$. Note that the rotor resistance at maximum torque point (near 43 $^{\circ}C$) in Fig. 2 is the effective rotor resistance used to design the MTPA control law in (11)-(12).

The effective rotor resistance calculated from $Y_r(s)$ in (10), ω_s^* =1.79 rad/s and T_e^* =150 Nm, is around $0.176\,\Omega$, which is very close to the value estimated by the proposed AQDM based rotor resistance estimator near 43 $^{\circ}C$. This indicates that the proposed estimator estimates the actual rotor resistance with higher accuracy than the CQDM based rotor resistance estimator which underestimates the actual rotor resistance.

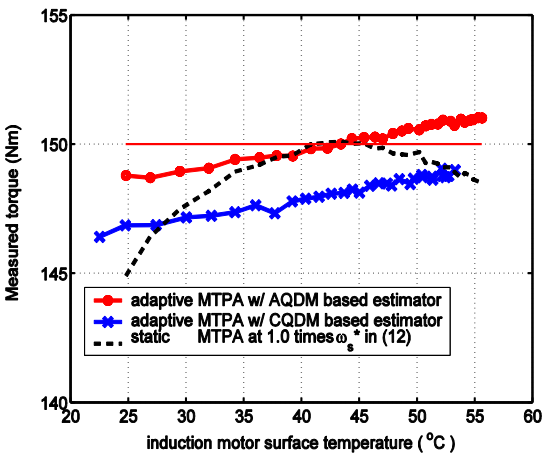

(a) Estimated torques at optimal slip frequencies.

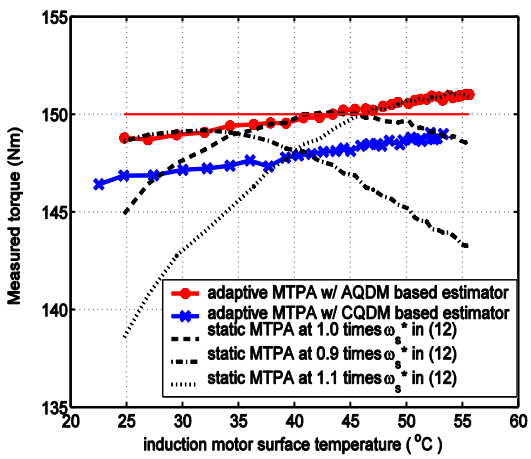

(b) Maximum torque per amp condition.

Fig. 6. Comparison of performances by the static MTPA control strategy and the adaptive MTPA control strategy at one operating condition.

7. Conclusion

It was experimentally shown that the MTPA control strategy performs sub-optimally unless rotor resistance variation due to rotor temperature change is taken into consideration. In order to maintain optimal performance of the MTPA control strategy, a new AQDM based rotor resistance estimator is proposed in this work. The proposed AQDM based rotor resistance estimator is designed to predict the rotor resistance regardless of operating conditions, since it takes magnetizing saturation and leakage path saturation into account.

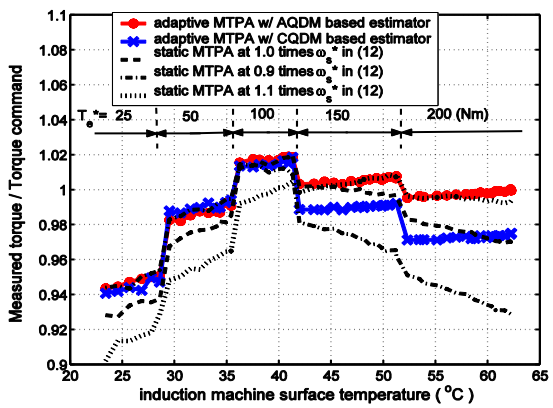

Fig. 7. Comparison of performances by static MTPA control strategy and the adaptive MTPA control strategy un der several operating conditions from light load to he avy load at 900 rpm rotor resistance estimator.

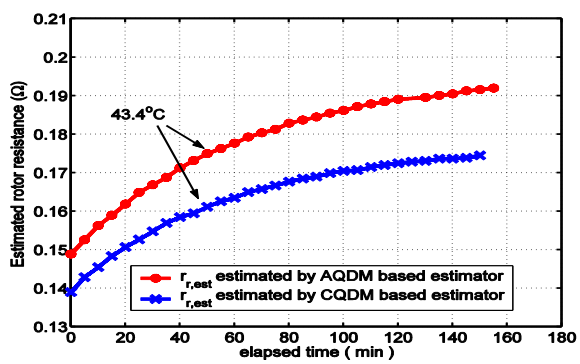

Fig. 8. Comparison of the estimated rotor resistance by the proposed rotor resistance estimator and the CQDM based rotor resistance estimator under one operating condition at 900 rpm with the torque command of 150 Nm.

The proposed AQDM based rotor resistance estimator was first validated using a computer simulation study that demonstrated that the estimator worked well during a series of transient events. Next, the performance of the proposed AQDM based rotor resistance estimator was experimentally demonstrated by its incorporation into an adaptive MTPA control. It was also compared to the performance of an adaptive MTPA control strategy in which the rotor resistance was determined from a CQDM based rotor resistance estimator. In particular, it was shown that the adaptive MTPA control with the proposed AQDM based rotor resistance estimator incorporated accurately achieved the desired torque regardless of torque command or surface temperature (and presumably rotor temperature). It was also shown that this was not the case for a static MTPA control or for an adaptive MTPA control strategy in which the rotor resistance was determined by a CQDM based rotor resistance estimator.

References

[1] B. karanavil, M.F. Rahman, and C. Grantham, "Implementation of an on-line resistance estimation using arfitificial neural networks for vector controlled induction motor drive," *The 29th Annual Conference of the IEEE Industrial Electronics Society*, Vol. 2, pp. 1703-1708, Nov., 2003.

[2] M. Benhaddadi, K. Yazid, and R. Khaldi, "An Effective Identification of Rotor Resistance for Induction Motor Vector Control," *IEEE Instrumentation and Measurement Technology Conference*, Vol. 1, pp. 339-342, May 1997.

[3] Y. Miloud and A. Draou, "Fuzzy Logic Based Rotor Resistance Estimator of an Indirect Vector Controlled Induction Motor Drive," IEEE Industrial Electronics Society, *IECON02*, Vol. 2, pp.961-966, Nov., 2002.

[4] M.A. Ouhrouche, "Vector Control of an Induction Motor With On-line Rotor Resistance Identification," *Proceedings of the 1999 IEEE Canadian Conference on Electrical and Computer Engineering Shaw Conference Center*, Edmonton, Alberta, Canada, pp. 1121-1125, May, 1999,

[5] F. Zidani, M.S. Nait-Said, M.E.H. Benbouzid, D. Diallo, and R. Abdessemed, "A Fuzzy Rotor Resistance Updating Scheme for an IFOC Induction Motor Drive," *IEEE Power Engineering Review*, pp. 47-50, Nov., 2001.

[6] S. Halasz, B.T. Huu, and K. Veszpremi, "Rotor Time Constant On-line Identification For Field Oriented AC Drive," *Proceedings of the IEEE International Symposium*,

Vol. 2, pp. 654-659, July 1995, pp. 654-659, 1995.

[7] C. Gonzalez, J. Arribas, and D. Prieto, " Optimal Regulation of Electric Drives With Constant Load Torque," *IEEE transactions on Industrial Electronics*, Vol. 53, No. 6, pp. 1762-1769, December 2006.

[8] G. Bartolini, A. Pisano, and P. Pisu, "Simplified Exponentially Convergent Rotor Resistance Estimation for Induction Motors," *IEEE Transactions on Automatic Control*, Vol. 48, No. 2, pp. 325-330, Feb., 2003.

[9] S.K. Jeong, Z.G. Lee, H.A. Toliyat, and P. Niazi, "Sensorless Control of Induction Motors With Simultaneous On-line Estimation Of Rotor Resistance and Speed Based on the Feedforward Torque Control Scheme," *IEEE International Electric Machines and Drives conference*, Vol. 3, pp. 1837-1842, June 2003.

[10] A. Miloudi and A. Draou, "Variable Gain PI Controller Design For Speed Control and Rotor Resistance Estimation of an Indirect Vector-controlled Induction Machine Drive," *IEEE 2002 28th Annual Conference of the Industrial Electronics Society*, Vol. 1, pp. 323-328, Nov., 2002,

[11] B. Karanayil, M. F. Rahman, and C. Grantham, " Online Stator and Rotor Resistance Estimation Scheme Using Artificial Neural Networks for Vector Controlled Speed Sensorless Induction Motor Drive," *IEEE transactions on Industrial Electronics*, Vol. 54, No. 1, pp. 167-176., February 2007.

[12] A. B. Proca and A. Keyhani, "Sliding-Mode Flux Observer With Online Rotor Parameter Estimation for Induction Motors," *IEEE transactions on Industrial Electronics*, Vol. 54, No. 2, pp. 716-723, April 2007.

[13] R. J. Kerkman, "Steady-state and transient analyses of an induction machine with saturation of the magnetizing branch," *IEEE Transactions on Industry Applications*, Vol. 21, No. 1, pp. 226-234, Jan/Feb, 1985.

[14] C. R. Sullivan, S. R. Sanders, "Models for induction machines with magnetic saturation of the main flux path," *IEEE Transactions on Industry Applications*, Vol. 31, No. 4, pp. 907-917, July/August, 1995.

[15] J. Langheim, "Modelling of rotorbars with skin effect for dynamic simulation of induction machines," *Conference Record of the 1989 IEEE Industry Applications Society Annual Meeting*, pp. 38-44, 1989.

[16] T. A. Lipo, A. Consoli, "Modeling of induction motors with saturable leakage reactances," *IEEE Transactions on Industry Applications*, Vol. 20, No. 1, pp. 180-189, Jan/Feb. 1984.

[17] A. C. Smith, R. C. Healey, S. Williamson, "A transient induction motor model including saturation and deep bar effect," *IEEE Transactions on Energy Conversion*, Vol. 11, No. 1, pp. 8-15, March, 1995.

[18] S. Moon, A. Keyhani, S. Pillutla, "Nonlinear neural-network modeling of an induction machine," *IEEE Transactions on Control Systems Technology*, Vol. 7, No. 2, pp. 203-211, March, 1999.

[19] C. Kwon, S. D. Sudhoff, "An Improved Maximum Torque Per Amp Control for Induction Machine Drives," in *20th Annual IEEE Applied Power Electronics Conference and Exposition*, pp. 740-745, March, 2005.

[20] S. D. Sudhoff, D. C. Aliprantis, B. T. Kuhn , and P. L. Chapman, "An Induction Machine Model for Predicting Inverter – Machine Interaction," *IEEE Transactions on Energy Conversion*, Vol. 17, pp. 203-210, June 2002.

[21] S. D. Sudhoff, P. L. Chapman, D. C. Aliprantis, and B. T. Kuhn, "Experimental Characterization of an Advanced Induction Machine Model," *IEEE Transactions on Energy Conversion*, Vol. 18, pp. 48-56, March 2003.

[22] C. Kwon, S. D. Sudhoff, "A Genetic Algorithm Based Induction Machine Characterization Procedure with Application to Maximum Torque Per Amp Control," *IEEE transaction on Energy Conversion*, Vol. 21, No. 2, June 2006.

[23] P. C. Krause, O. Wasynczuk, S. D. Sudhoff, Analysis of Electric Machinery and Drive Systems, IEEE Press, 2002.

[24] C. Kwon, S. D. Sudhoff, " An Adaptive Maximum Torque Per Amp Control Strategy," *the 2005 International Electric Machines and Drives Conference*, pp. 783-788, May 2005.

[25] P. L. Jansen and R. D. Lorenz, "A Physically Insightful Approach to the Design and Accuracy Assessment of Flux Observer for Field Oriented Induction Machine Drives," *IEEE Transactions on Industry Applications*, Vol. 30, No. 1, pp. 101-110, January/February 1994.

[26] J. Kim, J. Choi, and S. Sul, "Novel Rotor Flux Observer Using Observer Characteristic Function in Complex Vector Space for Field Oriented Induction Motor Drives," *IEEE transactions on Industry Applications*, Vol. 38, pp. 1334-1443, September/October 2002.

Chun-Ki Kwon received B.S. and M.S. degrees in Electrical Engineering from Korea University in 1992 and 1994, respectively. He is currently with Soonchunhyang University, Asan, Chunnam, Korea. His research interests include control and modeling of electric machines, especially related to medical engineering such as rehabilitation devices.